Efficient control of dye molecules fluorescence in polydopamine via strong optical coupling in a SPASER nanoparticle

Pavel Melentiev (melentiev@isan.troitsk.ru)
Institute of Spectroscopy Russian Academy of Sciences https://orcid.org/0000-0001-8958-453X
Boris Khlebtsov
Institute of Biochemistry and Physiology of Plants and Microorganism
Anton Gritchenko
Institute of Spectroscopy Russian Academy of Sciences
Denis Kudryavtsev
Shemyakin-Ovchinnikov Institute of Bioorganic Chemistry Russian Academy of Sciences
Igor Ivanov
Shemyakin-Ovchinnikov Institute of Bioorganic Chemistry Russian Academy of Sciences
Vera Mozhaeva
Shemyakin-Ovchinnikov Institute of Bioorganic Chemistry Russian Academy of Sciences
Andrei Siniavin
Shemyakin-Ovchinnikov Institute of Bioorganic Chemistry Russian Academy of Sciences
Bin Kang
Nanjing University
Victor Tsetlin
Shemyakin-Ovchinnikov Institute of Bioorganic Chemistry Russian Academy of Sciences
Victor Balykin
Institute of Spectroscopy Russian Academy of Sciences

Article

Keywords: dye molecules fluorescence, polydopamine, optical coupling, SPASER nanoparticle

Posted Date: June 8th, 2021

DOI: https://doi.org/10.21203/rs.3.rs-590449/v1

Efficient control of dye molecules fluorescence in polydopamine via strong optical coupling in a SPASER nanoparticle

P. Melentiev,[1,2] B. Khlebtsov,[3] A. Gritchenko,[1,2] D. Kudryavtsev,[4] I. Ivanov,[4] V. Mozhaeva,[4] A. Siniavin, [4,5] B. Kang,[6] V. Tsetlin,[4] V. Balykin[1,2]

[1]Institute of Spectroscopy RAS, Moscow 108840, Russia;

[2]Higher School of Economics, National Research University, Moscow 101000, Russia

[3]Institute of Biochemistry and Physiology of Plants and Microorganisms, Russian Academy of Sciences, 13 Prospekt Entuziastov, Saratov 410049, Russia

[4]Shemyakin-Ovchinnikov Institute of Bioorganic Chemistry of the RAS, Moscow 117997, Russia

[5]N.F. Gamaleya National Research Center for Epidemiology and Microbiology, Ivanovsky Institute of Virology, Ministry of Health of the Russian Federation, Moscow 123098, Russia

[6]State Key Laboratory of Analytical Chemistry for Life Science and Collaborative Innovation Center of Chemistry for Life Sciences, School of Chemistry and Chemical Engineering, Nanjing University, 163 Xianlin Road, Nanjing 210023, P. R. China

Abstract

One of the main approaches of design and manipulation of the quantum emitters' radiative properties is based on proper control of optical modes of the surrounding quantum emitter environment, leading to, in its ultimate case, to a strong regime of the emitter - environment interaction. In this Letter, we present the realization of a mesoscopic physical system (Au SPASER nanoparticle with polydopamine shell containing dye molecules Cy 7.5) in which the strong optical coupling regime allows: (i) to get rid of dye molecules quenching, (ii) to suppress photobleaching of dye molecules and (iii) to get a great enhancement of dye molecules fluorescence. We have reduced the rate of fluorescence quenching of dye molecules in PDA by 1000 times and increased the fluorescence emission rate of dye molecules by 30 time, thus preparing bright, nanoscale and biocompatible fluorescent probes suitable for bio-sensing applications. As an example of practical use of the probe, we demonstrate direct detection of single SARS-CoV-2 viral particle via fluorescence measurements of the probes attached to the viral particle through the antibodies.

1. Introduction

It is well known that the radiative properties of a quantum emitter (QE) can be controlled by the spatial and frequency distributions of the surrounding quantum emitter optical modes of the environment, leading to manifestation of weak, strong or ultra-strong coupling regimes of the emitter - environment interactions.[1] Photon density of states can be increased or reduced with respect to its free-space values, leading to inhibited or enhanced quantum emitter radiative properties, including QEs lifetime reduction, fluorescence enhancement, emission directivity and many other parameters.[2–5]

One of the possible ways to achieve light-matter coupling, the effects clearly related to the quantum electrodynamical types of interactions, is to couple the QE to the electromagnetic field in plasmonic cavity of metal nanoparticles.[3,6–11] In this case, coupling occurs when the QE is in resonance with the electromagnetic mode and the coupling strength dominates over the losses in the coupled system. As the interaction grows stronger, the regime of a weak coupling condition can be reached, demonstrating significant changes in the emission properties of QEs (the Purcell effect[12]).

When the coupling strength is increasing further, the `QE + photon mode' system reaches the strong coupling regime,[13] where the rate of coherent energy exchange between light and matter is higher than their decay rates. In the strong coupling regime, the energy states of the hybrid `QE + photon mode' system are split into two separate, so-called polaritonic states, with the energy separation between them being proportional to the coupling strength (the Rabi splitting).[13]

The coupling strength depends also on the number of QEs located in the optical cavity mode. Hence it can be further increased through arrangement of a large number of QEs in the cavity mode. In the case of plasmonic nanostructures used the optical cavity has a size much less than a wavelength of light, thus QE coherent collective interactions (the Dicke effect[14,15]) have to be taken into account. Such regime of coupling, related to the collective interactions, is characterized by the increased coupling strength compared to the non-collective case of the coupling; therefore, a very high-Q resonators are not anymore required to reach the strong coupling regime. The main fundamental and practical applications of strong coupling regime are due to the realization of a physical systems with the designed *radiation properties*.[13,16]

The first demonstration of strong coupling was realized using a high-Q optical resonator and neutral atoms.[17] However, with the plasmonic nanostructures, it is turned out much easier to get the condition of strong coupling

regime due to the small volume plasmon nanostructures' modes, which can be less than 10^3 nm^3.[18] To date, to create various hybrid nanoobject, plasmonic nanostructures of various geometries were used,[16] with different types of quantum emitters: dye molecules,[19] j-aggregates[20] or semiconductor quantum dots.[21] Note also existing applications of the hybrid nanosystems.[16,19]

In this work the main object of the study is PDA, polydopamine. PDAs are the most well-developed melanin mimicking materials possessing many attractive adhesive and optical properties such as antioxidant activity, high photothermal conversion efficiency[22] and strong metal ion chelation.[23–27] Moreover, PDA allows the possibility of formation a controllable shell on various nanostrustures.[28–30] Fluorescence property of material, as one of its important features widely used in medical imaging applications, has been less integrated in the PDA-based imaging platforms due to its extremely low quantum yield of the respected emission.[26,31] There were developed different approaches to solve this obstacle.[25] The first approach is based on a suppression of the dopamine (DA) polymerization or reduction of the π–π stacking interaction between the polymer chains in PDA, leading to appearance of PDA fluorescence but only in visible and UV spectral ranges. The problem still remains in the near-infra-red spectral range, which is specially suitable for ultrasensitive biological applications.[32] The numeral attempts to incorporate the fluorescent molecules inside of PDA are failed due to the quenching of molecules' fluorescence by PDA.[33,34] PDA was found to be a very efficient fluorescence quencher by Förster resonance energy transfer (FRET) and/or photoinduced electron transfer (PET) mechanisms, both affecting the fluorescence intensity of the attached dye molecules.[35–39] The quenching mechanism prevents the use of PDA as a host media for molecules to design nanolocalized sources with ultrabright emission. This problem remains unsolved today.

There is a huge progress in development and characterization of the so-called mesoscopic systems, the specific types of systems where due to their small size and design the manifestation of size-related effects takes place, including quantum – electrodynamics ones. In this paper we present results on the fabrication of a mesoscopic type system, formed by Au nanoparticle with polydopamine shell containing molecules Cy 7.5, in which strong optical coupling of dye molecules to plasmonic nanostructure helps get rid of the dye molecules quenching inside the PDA. Thus, it solved one of the long-known challenges of PDA material in photonics and in sensing applications. By introducing Cy 7.5 dye molecules inside a PDA shell, we realized nanoscale and biocompatible bright sources of near-infra-red emission and demonstrated application of created fluorescent probes for detection of single virus nanoparticles.

2. Strong optical coupling of dye molecules in PDA with plasmonic nanoparticle

In this work, the strong coupling regime is realized between a plasmonic Au nanostructure and Cy 7.5 dye molecules. Au nanostructure is in the form of a nanorod with a PDA shell containing Cy 7.5 dye molecules, Figure 1a. The nanorods have a 10 nm width and 40 nm length. At these geometrical parameters Au nanorod exhibit two plasmon resonances, at a wavelength of 510 nm (short-wavelength plasmon resonance, independent of the geometry of the nanorod) and in the near infrared range at 800 nm - 900 nm (long-wavelength resonance, wavelength dependent on ratio of the nanorod length to its diameter). The thickness of the PDA shell was chosen to be 10 nm.

The distinctive feature of the nanostructure studied in this work is an inclusion of a thin PDA layer containing dye molecules at high concentration. During the PDA shell growth Cy 7.5 dye molecules were embedded in polymeric shell at a concentration of 2.5×10^{18} cm^{-3}. Nanostructures having such a design are called in literature a SPASER nanoparticles. SPASER nanoparticles were first proposed[40] and experimentally investigated[41] in the works on the development of nanolocalized sources of coherent radiation (see a recent progress in the SPASER nanoparticles fabrications and applications[42–44]). The coherent emission from SPASER nanoparticles is realized only under high intensity of pumping-laser radiation. In this work we are not focusing on reaching the coherent emission from our SPASER nanoparticles but use quite moderate pumping-laser intensities, not sufficient to reach the coherent regime of respective emission.

The main idea behind SPASER nanoparticles is to compensate the losses of the plasmonic mode using an active medium. In this paper we do not focus on the effects of coherent radiation and use the SPASER nanoparticles design to reach optical strong coupling conditions. Note that the very design of SPASER nanoparticles, containing high concentrations of dye molecules in the small volume plasmonic mode, provides almost ideal conditions to study the strong coupling interactions. To the best of our knowledge the strong coupling manifestation in SPASER nanoparticles was not reported before.

The inset in Figure 1c shows the results of the FDTD (finite-difference time-domain method) calculation of the spatial distribution of the electrical field amplitude near the SPASER nanostructure when it is irradiated with monochromatic radiation at 850 nm wavelength having polarization directed along the SPASER Au nanorod. As can be seen from the figure, near the surface of the nanorod the field is enhanced due to the excitation of localized plasmon resonances. When dye molecules are arranged in the SPASER plasmonic mode, the two distinct scenarios

can be realized.[16] In the first one, known as the weak coupling regime, the excited dye molecules undergo exponential decay into the ground state, accompanied by spontaneous emission of photons. The presence of the cavity in this case modifies the local density of optical states and, according to the Fermi golden rule,[45] the resulting decay rate. In this particular case, the process of spontaneous decay may be calculated semiclassically, and the enhancement of the decay rate, known as the Purcell factor, can be computed from the electromagnetic Green tensor of the structure.[12,46–48]

In the second case, that is, at strong coupling regime, the coherent energy exchange between the QE and the cavity mode occurs. The rate of this exchange, Ω, is faster than any decay rates in the system, and thus the dynamics of the system is greatly different from the weak coupling case. To correctly describe the physics of a strongly coupled system, both the QE and the optical cavity mode should be quantized.[45] The single-mode cavity field is described by the standard Hamiltonian $\hbar\omega\hat{a}^{\dagger}\hat{a}$, where ω is the mode frequency and $\hat{a}$ is the photon annihilation operator. The emitter-cavity interaction is mediated via the electric dipole term, $\widehat{\boldsymbol{d}} \cdot \widehat{\boldsymbol{E}}(\boldsymbol{r}_d)$, where $\widehat{\boldsymbol{E}}(\boldsymbol{r}_d) = \mathcal{E}(\hat{a}^{\dagger} + \hat{a})$ is the electric field operator at the position of the emitter, $\widehat{\boldsymbol{d}} = \boldsymbol{d}_{eg}(\hat{\sigma} + \hat{\sigma}^{\dagger})$ is the QE dipole moment operator, and $\mathcal{E}$ is the vacuum electric field. In the commonly used rotating wave approximation the resulting Hamiltonian in the Jaynes-Cummings (JC) model can be written as:[16]

$$\widehat{\mathcal{H}} = \hbar\omega_0\hat{\sigma}^{\dagger}\hat{\sigma} + \hbar\omega\hat{a}^{\dagger}\hat{a} + \hbar g(\hat{\sigma}\hat{a}^{\dagger} + \hat{\sigma}^{\dagger}\hat{a}), \quad (1)$$

where g is the coupling constant given by $g = -\boldsymbol{d}_{eg}\mathcal{E}/\hbar$. The characteristic feature of the strong coupling regime is the Rabi splitting between the eigenstates of the hybrid system. It can be blurred out by spontaneous decay and dephasing in the system. The losses associated with incoherent processes can be described phenomenologically by introducing the complex energies of the QE, $\omega_0 - i\gamma$, and the cavity, $\omega - i\kappa$, where κ and γ are the cavity and emitter decay rates. The resulting eigen energies in the case of weak excitation, with a number of absorbed photons by the hybrid system less than one, may be found by diagonalizing the following non-Hermitian Hamiltonian (for greater number of absorbed photons, such an approach fails to describe eigenstates, and a rigorous dissipative approach is required instead[45]), with yields energies of the two states:

$$E_{\pm} = \frac{\omega+\omega_0}{2} - \frac{i}{2}(\gamma + \kappa) \pm \sqrt{g^2 + \frac{1}{4}\big(\delta - i(\gamma - \kappa)\big)^2} \quad (2)$$

where $\delta = \omega - \omega_0$ is the detuning. In the resonant case $\omega = \omega_0$, the Rabi splitting between these two states is

$\Omega = \sqrt{4g^2 - (\gamma - \kappa)^2}$. In order to spectrally resolve the two states, the Rabi splitting Ω must exceed the energy state full width at half-maximum, which in the notation of the above equation reads:[49–51] $\Omega > \gamma + \kappa$. Strong coupling is a distinct regime of light–matter interaction, when the Rabi frequency exceeds the rate of electromagnetic mode damping and the emitter decay rates. This regime of interaction manifests itself in coherent oscillations of energy between matter and photonic subsystem. In the frequency domain, this leads to modification of the spectroscopic response of the system such that two new normal modes emerge.

The Rabi splitting can be measured from the respective extinction spectra of hybrid system.[16,19] Figure 1c shows the dispersion energy diagram of a strongly coupled system: SPASER nanoparticles having Cy 7.5 molecules. On the vertical axis is the energy of resonance peaks; on the horizontal axis is the detuning of the long-wavelength plasmon resonance from the absorption frequency of Cy 7.5 dye molecules. Lines on the figure are fitting of the experimental points to the calculated values. The dispersion energy diagram yields the vacuum Rabi coupling strength of $\Omega \approx 148 \pm 5$ meV. The gray color around the black lines corresponds to the imaginary part of the energy of hybrid system with their width corresponding to the relaxation rate in the system. At points far from the anticrossing of LP and UP curves, the relaxation is characterized mainly by a dye (γ) or a plasmonic subsystem (κ) decay rates.

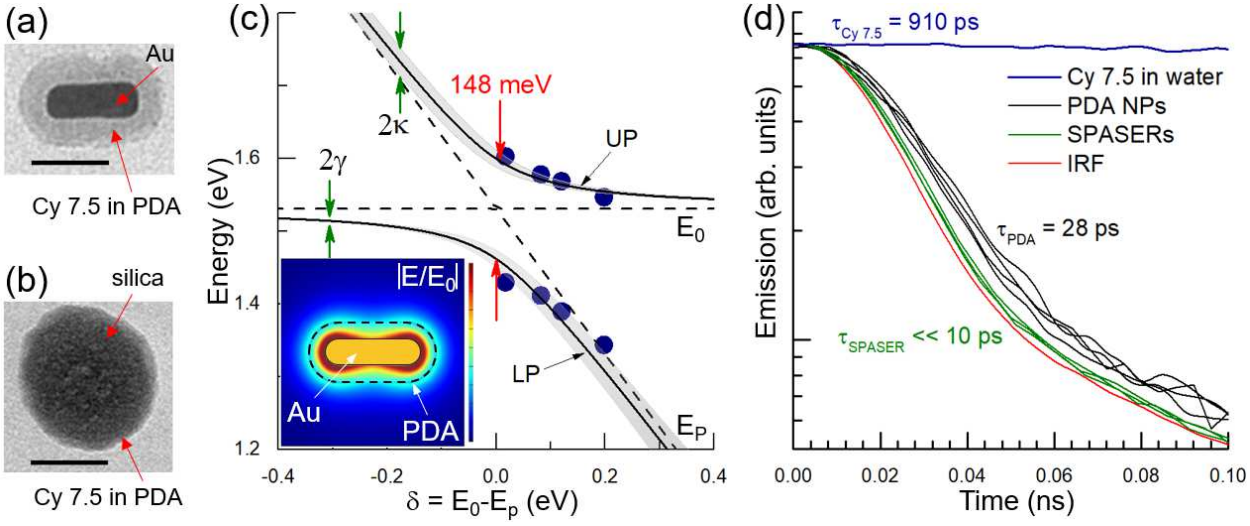

Figure 1| *SPASER and PDA samples and their characterization: (a) TEM of SPASER nanoparticle formed by Au nanorod and PDA shell containing molecules Cy 7.5. (b) TEM of a PDA nanoparticle formed by a silica sphere and PDA shell with Cy 7.5 molecules. (c) Dispersion energy diagram of a strongly coupled system - SPASER nanoparticle formed by Au nanorod and PDA shell with molecules Cy 7.5. Diagram shows: the eigen energies values versus detuning $\delta = E_0 - E_p$ between plasmon (E_p) and dye (E_0) resonances. Gray shadows around black lines related to the imaginary part of eigen energies (1) of hybrid system, which*

determines the rate of energy decay. Lines are fits to Rabi coupling model. The inset shows the results of the FDTD calculation of the electrical near-field amplitude when a SPASER nanostructure is irradiated with monochromatic radiation at 850 nm wavelength with polarization along the SPASER nanorod main axis. (d) Comparison of the decay rates of: (i) free Cy 7.5 dye molecules in water (red line), (ii) Cy 7.5 molecules in PDA nanostructure (black curves), (iii) SPASER nanoparticles (green curves), and (iv) impulse response function of the setup (IRF, red curve). Scale bars in TEM images are 30 nm.

Figure 1d shows the data of the fluorescence decay time measurements upon excitation by pulsed laser radiation having a 100 fs pulse duration for three different systems: (i) free Cy 7.5 dye molecules in water (red line), (ii) Cy 7.5 molecules in a PDA nanostructure (black curves), (iii) SPASER nanoparticles (green curves), impulse response function of the setup (IRF, red curve). The data show that the presence of dye molecules in the PDA shell leads to a decrease in the relaxation time from 910 ps to 28 ps, which is caused by the intrinsic PDA quenching mechanism. In the case of SPASER nanoparticles, the relaxation times turn out to be significantly shorter than 10 ps which is the minimum measurement time in the experimental setup. Such a short relaxation time of the dye fluorescence in this case is associated with the hybridization of the energy levels of the dye molecules with plasmon resonances, which leads to a large imaginary energy component in the anticrossing region, thus manifesting relaxation time value comparable to one of the plasmonic subsystem (see Figure 1c).

3. Effect of strong coupling on dye molecules fluorescence

Since the discovery of polydopamine (PDA) in 2007[52] it was believed that it is impossible to use of PDA as a host media for dye molecules due to strong quenching mechanism associated with Foerster resonance energy transfer (FRET) and/or photoinduced electron transfer (PET) mechanisms.[35–39] In the following we will show that this problem can be solved by the realization of a mesoscopic physical system (Au SPASER nanoparticle with polydopamine shell containing Cy 7.5 molecules) in which the strong optical coupling condition is realized.

As is well known, optical quenching can be influenced by the local photonic mode density and, accordingly, can be enhanced or attenuated using different types of resonators.[53] Thus, it has been shown that Fabry-Perot cavity[54] or a plasmonic nanoantenna[55] can be used to control the efficiency of FRET.

Here we for the first time demonstrate the possibility to control dye molecules quenching in PDA using the strong coupling of dye molecules with a plasmonic nanoparticle. The resulting exciton (dye molecules) - plasmon (nanostructure) hybridization can lead to cavity-induced emission of optically excited dye molecules, at times shorter than the characteristic times of fluorescence quenching by the PDA material.

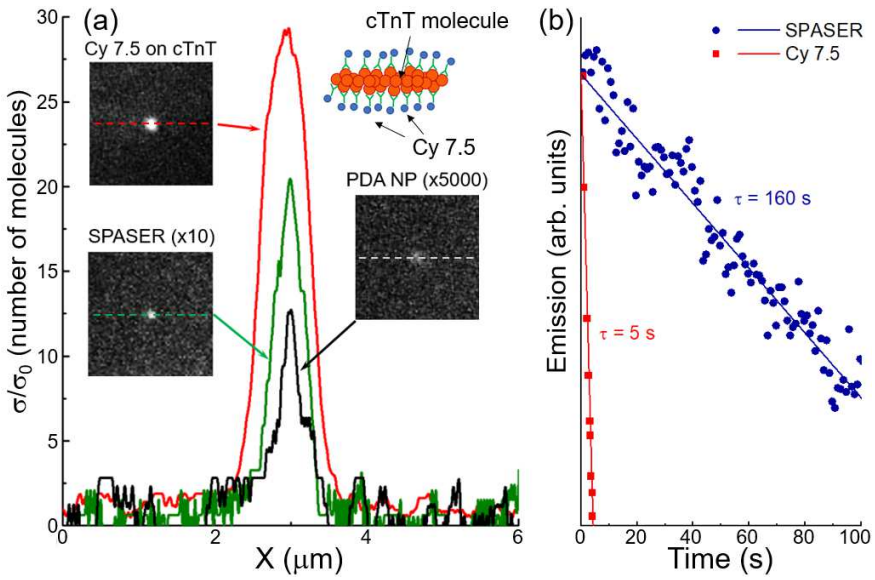

Figure 2| *Comparison of Cy 7.5 molecules emission in different samples: (a) fluorescence cross-sections* $\sigma = P_{emiss}/I_{Laser}$ *of a single SPASER nanoparticle (green), PDA nanoparticle (black) and a nanoscale complex formed by ~30 Cy 7.5 molecules attached by antibodies to a single cTnT molecule (red) (see inserted schematic). The fluorescent cross-sections are taken from CCD images (see inserts) and are normalized to the fluorescence cross-section* σ_0 *of a single Cy 7.5 molecule upon excitation by laser radiation at 780 nm wavelength. (b) Amplitude-normalized photobleaching dynamics of fluorescence of single SPASER nanoparticle in comparison with the fluorescence of Cy 7.5 dye molecules in water*.

The simplest case, the approach to reduce quenching is to form a new emissive channel for the excited state energy dissipation. Briefly, let us consider a dye molecule having radiation rate γ in vacuum. The probability to emit a photon by the excited molecule at a time interval t after the excitation is $p_{emiss} = \gamma t$. The time interval t much shorter than the corresponding spontaneous emission time. Since there are no other channels of the excited energy dissipation, then the excited state relaxation probability is $p_{relax} \equiv p_{emiss}$. If the molecule is arranged in the PDA medium, characterized by a probability p_{quench}^{PDA} of the energy transfer from a molecule excited state into other channels rather than emission, the total relaxation probability can be written as $p_{relax}^{DPA} = p_{emiss}^{PDA} + p_{quench}^{PDA}$. If $p_{emiss}^{PDA} \ll p_{quench}^{PDA}$, then the molecule is practically not emitting light. The realization of the storing coupling can dramatically change the p_{emiss}^{PDA} rate vs p_{quench}^{PDA} rate, since in this case the Rabi oscillations of energy between the molecule and a plasmonic particle are at much faster times compared to the PDA quenching rate. Indeed, as was shown above, the DPA quenching rate is characterized by a 28 ps relaxation time, while the emission decay time of SPASER nanoparticle is 10 ps, i.e is much shorter than quenching time, Figure 1c.

To analyze quantitatively the effect of strong coupling on the dye molecules emission, we performed the fluorescence measurement from various *single nanoobjects* excited by the laser radiation. Figure 2a shows such

measurements from the following nanoobjects: (1) PDA nanostructure: the core of the nanostructure is formed by a silica sphere, which is covered with a 5 nm PDA shell containing Cy 7.5 molecules; (2) plasmonic nanostructure: formed by an Au nanorod and a PDA shell containing Cy 7.5 molecules, (3) a nanoscale complex formed by ~30 Cy 7.5 molecules attached by antibodies to a single cTnT molecule.[32] The last nanoobject is used as a reference radiation source. The PDA shells of both SPASER nanoparticles and nanoparticles with a silica core contain about 1000 dye molecules, which corresponds to a volume concentration of about 2.5×10^{18} cm^{-3}. A continuous laser radiation with the intensity of about 1 kW/cm^2 was used to excite fluorescence in the abode listed objects.

The inserts in Figure 2a show the optical images of the studied nanoobjects made by using their laser excited fluorescence. The cross-sections of these images are shown in Figure 2a. The amplitudes of signals of Figure 2d curves were normalize to show the laser-excited-fluorescence process cross-section $\sigma = \mathrm{P_{emiss}}/\mathrm{I_{Laser}}$ (P_{emiss} – power of detected fluorescence, I_{Laser} – intensity of laser light) normalized to the signals of a single Cy 7.5 molecule. Such a normalization allows us to determine the effective number of emitting molecules in each of the nanoobjects. From the performed measurements, it can be seen that the brightest of the objects is a complex containing 30 dye molecules. The weakest fluorescence is observed from the PDA nanoparticle, which is explained by the quenching of the fluorescence of the dye molecules by polydopamine. In this case, the effective number of fluorescent dye molecules is substantially less than unity. From the data presented, it can be seen that quenching of luminescence by polydopamine is a rather effective process that suppresses luminescence from 1000 dye molecules by more than 10^5 times! In the SPASER nanoparticle, the fluorescence of dye molecules is almost 1000 times stronger in comparison with the PDA nanostructure and corresponds to the fluorescence of about 2 dye molecules. This is due to the realization of a strong optical coupling of the dye molecules with the plasmonic nanostructure in the SPASER nanoparticle.

Shown in Figure 1 - Figure 2a data demonstrates the implementation of strong optical coupling in SPASER nanoparticles, characterized by a rather large value of the Rabi splitting equals 148 meV. In this case, in the system of dye molecule - plasmon nanoparticle, forming a SPASER nanoparticle, energy transfer at Rabi frequencies occurs from the plasmon subsystem to the photon subsystem (dye molecule) and back corresponding to times significantly less than 10 ps. The energy transfer process associated with the PDA quenching mechanism turns out to be much slower, the relaxation time in this case equals 28 ps. This leads to a significant weakening of the effect of fluorescence quenching of dye molecules in PDA, which manifests itself in a significant increase of SPASER nanoparticles fluorescence in comparison with PDA nanoparticles (not having Au nanorod). Note that at the used

dye molecules concentrations, the number of Cy 7.5 molecules located in the plasmonic nanoparticle mode is small, less than 10. This explains the lower fluorescence intensity of SPASER nanoparticles in comparison with the complex of dye molecules on the cTnT molecule. Note that the direct comparison of the fluorescence of dye molecules (Cy 7.5 molecules on cTnT) and dye molecules in the strong coupling regime is a rather complicated task, including the needs to take into account the change in the relaxation time in the system, as well as the change in the excitation probability associated with changing the saturation intensity of the optical transition.

Among the known emitters of light, dye molecules are the most popular in many photonics applications due to high quantum yield and low price.[56] Photobleaching is the biggest known disadvantage of dye molecules, leading to a limited number of emitted photons from individual molecules and thus limiting their applications. The photobleaching mechanism is related to photodynamic interactions between the excited triplet state of dye molecules and atmospheric triplet oxygen ($^3O_2$). It is known that most of dye molecules are characterized by a significant population transfer from the excited singlet state (S_1) to the long-lived triplet state (T_1). Due to a long lifetime of the triplet state, the molecules being excited in this state can interact with environmental oxygen and thus undergo photobleaching. The interaction between molecular oxygen and a dye molecule in triplet excitons can also lead to generation of several reactive oxygen species, such as singlet oxygen ($^1O_2$) and hydrogenperoxide (H_2O_2), which are highly unstable and therefore can chemically damage a dye molecule itself.[57,58] The known attempts to prevent photobleaching include the use of inert ambient as well as oxygen scavenger reagents,[59] and also the use of plasmonic nanoparticles for quenching of organic dye long-lived triplet states.[60–62]

When dye molecules are inside of a resonant cavity, the relaxation pathways and therefore photobleaching may be drastically modified. In the strong coupling limit, the photonic and excitonic components of the system cannot be treated as separate entities, as they form new polaritonic eigenstates (exciton-polaritons) having both light and matter characteristics. Recently, it has been demonstrated that not only optical but also material-related properties, such as chemical reactivity and charge transport, may be significantly altered in the strong coupling regime of light-matter interactions. It was show that a nanoscale system, composed of a plasmonic nanoparticle strongly coupled to excitons in a J-aggregated formed from organic chromophores, experiences modified excited-state dynamics and, therefore, modified photochemical reactivity.[20] Thus realized, in this scenario the probability to populate the long-lived triplet state becomes much smaller, leading to a dramatic reduction of the photobleaching rate. However, the effect of strong coupling on the molecules photobleaching was realized with j-

aggregates only, characterized by a large dipole moment and hence commonly used to build hybrid systems. However, the potential of strong coupling for photostability of organic dye molecules has not been explored.

Figure 2b shows the results of measurements of the photodegradation of single SPASER nanoparticles deposited on the quartz surface. The measurements were carried out by irradiating nanoparticles with CW laser radiation with an intensity of about 1 kW/cm^2. As a reference, the figure shows the data on photodegradation of free dye molecules in water. It can be seen from the figure that the stabilization of the photodegradation process is observed in SPASER nanoparticles, by analogy with the known data on the stabilization of radiation in j-aggregates.[20]

The effect of Cy 7.5 dye molecules stabilization presented in Figure 2b has a direct connection to one realized in experiments with j-aggregates.[20] Thus the probability to populate the long-lived triplet state of Cy 7.5 dye molecules, the state responsible for a photobleaching chemical reaction, becomes much smaller when strong coupling limits are reached. This leads to the measured a 30-folds reduction of the photobleaching rate.

Single viral particle detection

The measurements on SPASER nanoparticles formed with use of PDA shell with dye molecules (Figure 1 - Figure 2) have shown that they are an effective source of nanolocalized radiation with a photon flux about 2 times greater than can be obtained from a single dye molecule at the used excitation laser light intensity. Larger flux of photons from such source makes it possible to use them as nanoprobes with a 2 times larger signal to noise ratio. Moreover, the photostability of SPASER nanoparticles is approximately 30 times higher than that of free dye molecules, helping even further to increase the photon flux. A bright source of nanolocalized radiation used with a nanoprobe attached to biomolecules allows their detection at ultra-low concentrations. The measured concentration can be at the level of 10^7 molecules in 1 mL.[32] The method is based on attaching a large number (up to 27) of fluorescent molecules to biomolecule using antibodies with the following detection of the fluorescence of dye molecules attached-through-antibodies. The approach permits to visualize single biomolecules and trace their trajectory in solution. The method also allows measurements of ultra-low molecular concentrations by counting individual molecules, which is important for analytical applications. There are no visible obstacles of the method's applicability for ultra-fast, ultra-sensitive detection, monitoring, and imaging of other biological objects including pathogenic viruses and bacteria.

In this work, on the example of detecting SARS-CoV-2 viral particles, we show that the use of SPASER nanoparticles makes it possible to register significantly lower analyte concentrations, at the level of 10^3 - 10^4 particles per mL. Such low concentration of viral particles is the minimal detected concentration to date of serological fluid from patients infected with SARS-CoV-2 virus without the use of the pre-concentration steps.[63]

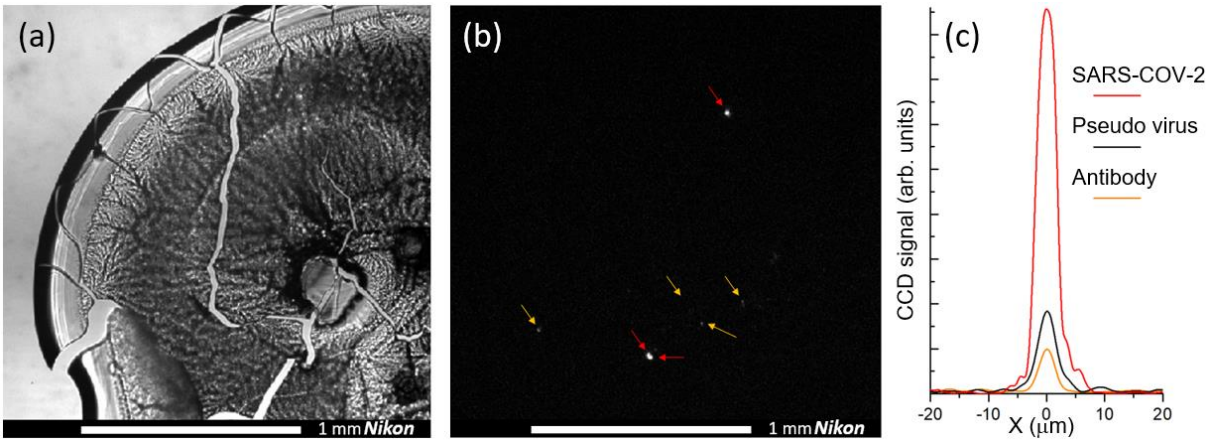

Figure 3| *Detection of single SARS-CoV-2 viral particles via measurement of SPASER nanoparticles fluorescence attached to virions through SARS-CoV-2 antibodies: (a) white-light image of dried out a droplet with added SPASER nanoparticles into it; (b) fluorescent image of the same droplet under 780 nm laser light excitation, orange arrows indicate antibodies' agglomerates, red arrows indicates SARS-CoV-2 viral particles; (c) cross-sections of fluorescent images of antibodies agglomerates (orange line), pseudo viral particle, having about 5 time less number of spike molecules (black line), SARS-CoV-2 viral particle (red line).*

The SARS-CoV-2 viral particle is characterized by the presence of spike-shaped S-proteins on the surface of its lipid membrane, for which they are often called spikes. The number of spikes on a surface of a single SARS-CoV-2 viral particle can be from 20 to 40.[64–66] In our work, SPASER nanoparticles were functionalized with antibodies to the SARS-CoV-2 S-spike using the well-known protocol for functionalization of the polydopamine surface.[67] At a sufficiently high concentration of SPASER nanoparticles in a sample containing SARS-CoV-2 viral particles, SPASER nanoparticles can be attached to the spike of viral particles through antibodies in a fairly large amount. Measurement of the fluorescence of SPASER nanoparticles located on a viral particle makes it possible to detect even single virions directly.

The samples containing SARS-CoV-2 strain hCoV-19/Russia/Moscow_PMVL-3 (GISAID ID: EPI_ISL_4708987) was isolated from an infected individual using Vero E6 cells (ATCC CRL-1586) in biosafety level-3 (BSL-3) facility. For optical measurements SARS-CoV-2 viral particles were inactivated by treatment with 0.5% formaldehyde solution. Pseudoviral SARS-CoV-2 particles were generated as described in ref.[68]. Briefly, 293T cells were transfected with 10 μg pLVPG (encoding the GFP), 8 μg pCMV-dR8.2 and 5μg pVAX1-S (encoding the SARS-CoV-2 Wuhan-Hu-1 spike

protein) using the transfection reagent Transporter 5 according to the manufacturer's instructions. The cell supernatant containing SARS-CoV-2 pseudo-typed virus was collected at day 3 after transfection, centrifuged to remove cellular debris, aliquoted and frozen at −80 °C. The SARS-CoV-2 pseudo-typed virus preparation was quantified using 293T/ACE2 cells.[69]

Anti-RBD monoclonal antibody was generated as described previously in ref.[70]. PDA coating of SPASER nanoparticles was made in the presence of ethylenediamine (1 mole%) to incorporate free amino groups, which later was used to covalently cross-link antibodies. To attach antibodies covalently to SPASER particles the following procedure was acquired. Freshly prepared SPASER nanoparticles were suspended in 50 mM $NaHCO_3$, then 50 mM solution of succinic anhydride in acetonitrile was added. The resulting mixture was shaken for 8 h, then succinyl-NPs were centrifuged, washed twice with 50% acetonitrile, then re-suspended in the activation buffer (50 mM MES pH 5.8 in 50% acetonitrile). Sulfo-NHS and EDT were added to the suspension of nanoparticles to the final concentration 10 mM. The mixture was shaken for 30 min, then centrifuged and the solution of protein in PBS was added immediately to the residue of activated NP. The resulting suspension was allowed to shake for 8 h at +4 C, then centrifuged, washed with 25 mM ethanolamine in PBS, followed by PBS washes. The resulting NP can be stored in PBS at +4 C for at least two weeks.

Figure 3a shows the CCD image from optical microscope under the white-light illumination of a dried drop to which SPASER-antibody nanoparticles have been added. Figure 3b shows a fluorescent optical image (in spectral range 800 nm - 900 nm) of the same sample of Figure 3a when the sample was irradiated by laser light (780 nm, intensity about 5 kW/cm^2). Several bright and weak spots (marked with arrows) are visible in the image. Our measurements showed that weak spots (marked with orange arrows) correspond to agglomerates of SPASER nanoparticles. Similar spots are observed in control samples with SPASER nanoparticles, but without SARS-CoV-2 viral particles. Each bright spot in Figure 3b (marked with red arrows) corresponds to the fluorescence of SPASER nanoparticles attached through antibodies to SARS-CoV-2 single viral particle. We estimate that approximately 20 SPASER nanoparticles are in each bright spot. These bright spots of fluorescence indicate the presence of viral particles in the SARS-CoV-2 sample. In samples without SARS-CoV-2 viral particles, as well as in samples with other types of viral particles (we also made the control measurements of the bovine coronavirus viral particles, not presented in the article), such bright spots were not recorded.

The presence of a large number of spikes of the SARS-CoV-2 viral particle allows the formation of a brightly fluorescent agglomerate consisting of about 20 SPASER nanoparticles. In control measurements, we used synthesized pseudoviral particles containing on average only 3 - 4 spikes, compared to 30 – 70 spikes on SARS-CoV-2 viral particle. In these measurements, the amplitude of the fluorescence signal from SPASER nanoparticles attached through antibodies in the pseudoviral particle was approximately 5 times smaller, in comparison with the corresponding signals when detecting SARS-CoV-2 viral particles. Cross-sections of the corresponding optical images are shown in Figure 3c. As it can be seen from the image the fluorescence signal from the pseudoviral particle is just 50% higher in amplitude compare to the fluorescence signal from the antibody agglomerate.

It is important to note that the measured high signal-to-noise ratio from SARS-CoV-2 viral particles (Figure 3c) is realized without using a special procedure for washing off antibodies unbound to viral particles. This is due to the fact that the substrate on which the drop was applied is functionalized with glutaraldehyde (a protein cross-linker) and osmium tetroxide (a lipid cross-linker) which fixes the SARS-CoV-2 viral particle to the substrate. When the droplets are becoming dry, the SPASER nanoparticles that have not bound with SARS-CoV-2 viral particles rush to the edge of the droplet - the well-known “coffee ring” effect when the droplet dries. The resulting low concentration of unbound SPASER nanoparticles in the central region of the droplet provides the obtained high signal-to-noise ratio in measurements of Figure 3c.

Conclusion

For the first time, we present the efficient method of dye molecules fluorescence control via strong optical coupling. The method allows: (i) to get rid of dye molecules quenching, (ii) to suppress photobleaching of dye molecules and (iii) to get a great enhancement of dye molecules fluorescence. Demonstration of the method is carried out on a mesoscopic system of Au SPASER nanoparticle with polydopamine (PDA) shell containing Cy 7.5 molecules in which a strong optical coupling of the dye molecules with the plasmonic nanoparticle occurs. We have shown that the realization of a strong optical coupling makes it possible to weaken the fluorescence quenching by a factor of about 1000. In addition, it was found that a strong optical coupling makes it possible a 30-fold suppression of the dye molecules photodegradation chemical reaction. We have shown the applicability of the developed method for a practically significant challenging task: the detection of single SARS-COV-2 virus nanoparticles.

We believe that the developed method is of a broader interest in the field of creating biocompatible and spectrally bright nanolocalized light sources for visualization of single biomolecules and biological objects, as well as in the sensorics of ultra-low concentrations of biomarkers used in the diagnosis of various diseases.

We thank N. Antipova, M. Pavliukov and M. Shahparonov for providing the anti-RBD antibody. This work was supported by the Russian Foundation for Basic Research (contracts no. 19-02-00207, 20-32-90070, 20-02-00059, 20-04-60277). The strong coupling measurements were conducted with the financial support of the Russian Science Foundation (contract no. № 21-72-30018).

Author Contributions

P.M. performed optical measurements, and prepared the first draft of the paper; B.Kh. designed and fabricated SPASER and PDA samples; A.G. performed time decay measurements; D.K., I.I., V.M. performed samples for experiments with virions detection as well as developed sample preparation method; A.S. performed samples with virions; B.K. designed SPASER samples, V.Ts. and V.B. supervised the project. All authors edited the manuscript and participated in discussion of the content.

Competing Interests

The authors declare no competing financial interests.

References

1. Haroche, S. & Raimond, J. M. *Exploring the Quantum: Atoms, Cavities, and Photons*. *Exploring the Quantum: Atoms, Cavities, and Photons* (Oxford University Press, 2010). doi:10.1093/acprof:oso/9780198509141.001.0001.

2. Anger, P., Bharadwaj, P. & Novotny, L. Enhancement and Quenching of Single-Molecule Fluorescence Optomechanics with levitated nanoparticles. *Phys. Rev. Lett.* **96**, 113002 (2006).

3. Hoang, T. B. *et al.* Ultrafast spontaneous emission source using plasmonic nanoantennas. *Nat. Commun.* **6**, 1–7 (2015).

4. Bouchet, D. *et al.* Enhancement and Inhibition of Spontaneous Photon Emission by Resonant

Silicon Nanoantennas. *Phys. Rev. Appl.* **6**, 064016 (2016).

5. Agranovich, V., Benisty, H. & Weisbuch, C. Organic and inorganic quantum wells in a microcavity: Frenkel-Wannier-Mott excitons hybridization and energy transformation. *SolidState Commun.* **102**, 631–636 (1997).

6. Greffet, J. J. Nanoantennas for light emission. *Science (80-.).* **308**, 1561–1563 (2005).

7. Kühn, S., Håkanson, U., Rogobete, L. & Sandoghdar, V. Enhancement of single-molecule fluorescence using a gold nanoparticle as an optical nanoantenna. *Phys. Rev. Lett.* **97**, 017402 (2006).

8. Pfeiffer, M. *et al.* Enhancing the optical excitation efficiency of a single self-assembled quantum dot with a plasmonic nanoantenna. *Nano Lett.* **10**, 4555–4558 (2010).

9. Busson, M., Rolly, B., Stout, B., Bonod, N. & Bidault, S. Accelerated single photon emission from dye molecule-driven nanoantennas assembled on DNA. *Nat. Commun.* **3**, 1–6 (2012).

10. Acuna, G. *et al.* Fluorescence Enhancement at Docking Sites of DNA-Directed Self-Assembled Nanoantennas. *Science (80-.).* **338**, 506–510 (2012).

11. Bidault, S. *et al.* Picosecond Lifetimes with High Quantum Yields from Single-Photon-Emitting Colloidal Nanostructures at Room Temperature. *ACS Nano* **10**, 4806–4815 (2016).

12. Purcell, E. M., Torrey, H. C. & Pound, R. V. Resonance absorption by nuclear magnetic moments in a solid. *Physical Review* vol. 69 37–38 (1946).

13. Tame, M. S. *et al.* Quantum plasmonics. *Nat. Phys.* **9**, 329–340 (2013).

14. Dicke, R. H. The effect of collisions upon the doppler width of spectral lines. *Phys. Rev.* **89**, 472–473 (1953).

15. Budker, D., Kimball, D., Kimball, D. F. & DeMille, D. P. *Atomic physics: an exploration through problems and solutions*. (Oxford University Press, 2004).

16. Baranov, D. G., Wersall, M., Cuadra, J., Antosiewicz, T. J. & Shegai, T. Novel Nanostructures and Materials for Strong Light-Matter Interactions. *ACS Photonics* **5**, 24–42 (2018).

17. Thompson, R. & Rempe, G. Observation of normal-mode splitting for an atom in an optical cavity. *Phys. Rev. Lett.* **68**, 1132 (1992).

18. Bozhevolnyi, S. I. & Khurgin, J. B. The case for quantum plasmonics. *Nat. Photonics* **11**, 398–400 (2017).

19. Dovzhenko, D., Ryabchuk, S., Rakovich, Y. & Nabiev, I. Light–matter interaction in the strong coupling regime: configurations, conditions, and applications. *Nanoscale* **10**, 3589–3605 (2018).

20. Munkhbat, B., Wersäll, M., Baranov, D. G., Antosiewicz, T. J. & Shegai, T. Suppression of photo-oxidation of organic chromophores by strong coupling to plasmonic nanoantennas. *Sci. Adv.* **4**, eaas9552 (2018).

21. Santhosh, K., Bitton, O., Chuntonov, L. & Haran, G. Vacuum Rabi splitting in a plasmonic cavity at the single quantum emitter limit. *Nat. Commun.* **7**, 1–5 (2016).

22. Kim, S. H. *et al.* Photothermal conversion upon near-infrared irradiation of fluorescent carbon nanoparticles formed from carbonized polydopamine. *RSC Adv.* **6**, 61482–61491 (2016).

23. Liu, Y., Ai, K. & Lu, L. Polydopamine and its derivative materials: Synthesis and promising applications in energy, environmental, and biomedical fields. *Chemical Reviews* vol. 114 5057–5115 (2014).

24. Liu, M. *et al.* Recent Development of Polydopamine: An Emerged Soft Matter for Surface Modification and Biomedical Applications Received. *Nanoscale* **8**, 16819–16840 (2016).

25. Zou, Y. *et al.* Synthetic Melanin Hybrid Patchy Nanoparticle Photocatalysts. *J. Phys. Chem. C* **123**, 5345–5352 (2019).

26. Yang, P., Zhang, S., Chen, X., Liu, X. & Wang, Z. Recent developments in polydopamine fluorescent nanomaterials. *Mater. Horizons* **7**, 746–761 (2019).

27. Yang, P. *et al.* Tailoring Synthetic Melanin Nanoparticles for Enhanced Photothermal Therapy. *ACS Appl. Mater. Interfaces* **11**, 42671–42679 (2019).

28. Zeng, Y., Liu, W., Wang, Z., Singamaneni, S. & Wang, R. Multifunctional Surface Modification of Nanodiamonds Based on Dopamine Polymerization. *Langmuir* **34**, 4036–4042 (2018).

29. Park, J. *et al.* Polydopamine-based simple and versatile surface modification of polymeric nano drug carriers. *ACS Nano* **8**, 3347–3356 (2014).

30. Black, K. C. L., Yi, J., Rivera, J. G., Zelasko-Leon, D. C. & Messersmith, P. B. Polydopamine-enabled surface functionalization of gold nanorods for cancer cell-targeted imaging and photothermal therapy. *Nanomedicine* **8**, 17–28 (2013).

31. Meredith, P. & Riesz, J. Radiative Relaxation Quantum Yields for Synthetic Eumelanin¶. *Photochem. Photobiol.* **79**, 211–216 (2007).

32. Melentiev, P. N. *et al.* Ultrafast, Ultrasensitive Detection and Imaging of Single Cardiac Troponin-T Molecules. *ACS Sensors* **5**, 3576–3583 (2020).

33. Dong, Z. *et al.* Polydopamine nanoparticles as a versatile molecular loading platform to enable imaging-guided cancer combination therapy. *Theranostics* **6**, 1031 (2016).

34. Wang, C. *et al.* Skin Pigmentation-Inspired Polydopamine Sunscreens. *Adv. Funct. Mater.* **28**, 1802127 (2018).

35. Ma, S. *et al.* Selective and sensitive monitoring of cerebral antioxidants based on the dye-labeled DNA/polydopamine conjugates. *Anal. Chem.* **88**, 11647–11653 (2016).

36. Fan, D. *et al.* A polydopamine nanosphere based highly sensitive and selective aptamer cytosensor with enzyme amplification. *Chem. Commun.* **52**, 406–409 (2016).

37. Qiang, W., Li, W., Li, X., Chen, X. & Xu, D. Bioinspired polydopamine nanospheres: A superquencher for fluorescence sensing of biomolecules. *Chem. Sci.* **5**, 3018–3024 (2014).

38. Ji, X. *et al.* On the pH-dependent quenching of quantum dot photoluminescence by redox active

dopamine. *J. Am. Chem. Soc.* **134**, 6006–6017 (2012).

39. Medintz, I. L. *et al.* Quantum-dot/dopamine bioconjugates function as redox coupled assemblies for in vitro and intracellular pH sensing. *Nat. Mater.* **9**, 676–684 (2010).

40. Bergman, D. & Stockman, M. Surface Plasmon Amplification by Stimulated Emission of Radiation: Quantum Generation of Coherent Surface Plasmons in Nanosystems. *Phys. Rev. Lett.* **90**, 027402 (2003).

41. Noginov, M. A. *et al.* Demonstration of a spaser-based nanolaser. *Nature* **460**, 1110–1112 (2009).

42. Wang, J. H. *et al.* How Gain layer design determines performance of nanoparticle-based spaser. *J. Phys. Chem. C* **124**, 16553–16560 (2020).

43. Song, P. *et al.* Three-level spaser for next-generation luminescent nanoprobe. *Sci. Adv.* **4**, eaat0292 (2018).

44. Gao, Z. *et al.* Spaser Nanoparticles for Ultranarrow Bandwidth STED Super-Resolution Imaging. *Adv. Mater.* **32**, 1907233 (2020).

45. Scully, M. & Zubairy, M. *Quantum optics*. (Cambridge University Press, 1997).

46. Pelton, M. Modified spontaneous emission in nanophotonic structures. *Nat. Photonics* **9**, 427−435 (2015).

47. Novotny, L. & Van Hulst, N. Antennas for light. *Nat. Photonics* **5**, 83–90 (2011).

48. Russell, K. J., Liu, T. L., Cui, S. & Hu, E. L. Large spontaneous emission enhancement in plasmonic nanocavities. *Nat. Photonics* **6**, 459–462 (2012).

49. Khitrova, G., Gibbs, H. M., Kira, M., Koch, S. W. & Scherer, A. Vacuum Rabi splitting in semiconductors. *Nat. Phys.* **2**, 81–90 (2006).

50. Savasta, S. *et al.* Nanopolaritons: Vacuum rabi splitting with a single quantum dot in the center of a dimer nanoantenna. *ACS Nano* **4**, 6369–6376 (2010).

51. Väkeväinen, A. I. *et al.* Plasmonic surface lattice resonances at the strong coupling regime. *Nano Lett.* **14**, 1721–1727 (2014).

52. Lee, H., Dellatore, S. M., Miller, W. M. & Messersmith, P. B. Mussel-inspired surface chemistry for multifunctional coatings. *Science (80-.).* **318**, 426–430 (2007).

53. Kongsuwan, N. *et al.* Suppressed Quenching and Strong-Coupling of Purcell-Enhanced Single-Molecule Emission in Plasmonic Nanocavities. *ACS Photonics* **5**, 186–191 (2018).

54. Andrew, P. & Barnes, W. L. Förster energy transfer in an optical microcavity - Google Scholar. *Science (80-.).* **290**, 785–788 (2000).

55. Garcia-Parajo, M. F., Mivelle, M., Sanz-Paz, M., Wenger, J. & van Hulst, N. F. Nanoscale control of single molecule Förster resonance energy transfer by a scanning photonic nanoantenna. *Nanophotonics* **9**, 4021–4031 (2020).

56. Mycek, M. & Pogue, B. *Handbook of biomedical fluorescence*. (CRC Press, 2003).

57. Levitus, M. & Ranjit, S. Cyanine dyes in biophysical research: the photophysics of polymethine fluorescent dyes in biomolecular environments. *Q. Rev. Biophys.* **44**, 123 (2011).

58. Zheng, Q., Jockusch, S., Zhou, Z. & Blanchard, S. C. The Contribution of Reactive Oxygen Species to the Photobleaching of Organic Fluorophores. *Photochem. Photobiol.* **90**, 448–454 (2014).

59. Rasnik, I., McKinney, S., Methods, T. H.-N. & 2006, U. Nonblinking and long-lasting single-molecule fluorescence imaging. *Nat. Methods* **3**, 891–893 (2006).

60. Hale, G. D., Jackson, J. B., Shmakova, O. E., Lee, T. R. & Halas, N. J. Enhancing the active lifetime of luminescent semiconducting polymers via doping with metal nanoshells. *Appl. Phys. Lett.* **78**, 1502–1504 (2001).

61. Phane Ké Na-Cohen, S. *et al.* Plasmonic Sinks for the Selective Removal of Long-Lived States. *ACS Publ.* **5**, 9958–9965 (2011).

62. Manjavacas, A. *et al.* Magnetic Light and Forbidden Photochemistry: The Case of Singlet Oxygen.

J. Mater. Chem. C **5**, 11824–11831 (2017).

63. Barauna, V. G. *et al.* Ultrarapid On-Site Detection of SARS-CoV-2 Infection Using Simple ATR-FTIR Spectroscopy and an Analysis Algorithm: High Sensitivity and Specificity. *Anal. Chem.* **93**, 2950–2958 (2021).

64. Ke, Z. *et al.* Structures and distributions of SARS-CoV-2 spike proteins on intact virions. *Nat. 2020 5887838* **588**, 498–502 (2020).

65. Yao, H. *et al.* Molecular Architecture of the SARS-CoV-2 Virus. *Cell* **183**, 730-738.e13 (2020).

66. Turoňová, B. *et al.* In situ structural analysis of SARS-CoV-2 spike reveals flexibility mediated by three hinges. *Science (80-.).* **370**, 203–208 (2020).

67. Gu, G. E. *et al.* Fluorescent polydopamine nanoparticles as a probe for zebrafish sensory hair cells targeted in vivo imaging. *Sci. Rep.* **8**, 1–8 (2018).

68. Siniavin, A. E. *et al.* Snake venom phospholipases A2 possess a strong virucidal activity against SARS-CoV-2 in vitro and block the cell fusion mediated by spike glycoprotein interaction with the ACE2 receptor. *biorxiv.org* (2021) doi:10.1101/2021.01.12.426042.

69. Byazrova, M. *et al.* Pattern of circulating SARS-CoV-2-specific antibody-secreting and memory B-cell generation in patients with acute COVID-19. *Clin. Transl. Immunol.* **10**, e1245 (2021).

70. Antipova, N. V *et al.* Establishment of Murine Hybridoma Cells Producing Antibodies against Spike Protein of SARS-CoV-2. *Int. J. Mol. Sci. Artic.* **21**, 9167 (2020).

Figure Legends

Figure 1. SPASER and PDA samples and their characterization: (a) TEM of SPASER nanoparticle formed by Au nanorod and PDA shell containing molecules Cy 7.5. (b) TEM of a PDA nanoparticle formed by a silica sphere and PDA shell with Cy 7.5 molecules. (c) Dispersion energy diagram of a strongly coupled system - SPASER nanoparticle formed by Au nanorod and PDA shell with molecules Cy 7.5. Diagram shows: the eigen energies values versus detuning $\delta = E_0 - E_p$ between plasmon (E_p) and dye (E_0) resonances. Gray shadows around black lines related to the imaginary part

of eigen energies (1) of hybrid system, which determines the rate of energy decay. Lines are fits to Rabi coupling model. The inset shows the results of the FDTD calculation of the electrical near-field amplitude when a SPASER nanostructure is irradiated with monochromatic radiation at 850 nm wavelength with polarization along the SPASER nanorod main axis. (d) Comparison of the decay rates of: (i) free Cy 7.5 dye molecules in water (red line), (ii) Cy 7.5 molecules in PDA nanostructure (black curves), (iii) SPASER nanoparticles (green curves), and (iv) impulse response function of the setup (IRF, red curve). Scale bars in TEM images are 30 nm.

Figure 2. Comparison of Cy 7.5 molecules emission in different samples: (a) fluorescence cross-sections $\sigma = P_{emiss}/I_{Laser}$ of a single SPASER nanoparticle (green), PDA nanoparticle (black) and a nanoscale complex formed by ~30 Cy 7.5 molecules attached by antibodies to a single cTnT molecule (red) (see inserted schematic). The fluorescent cross-sections are taken from CCD images (see inserts) and are normalized to the fluorescence cross-section σ_0 of a single Cy 7.5 molecule upon excitation by laser radiation at 780 nm wavelength. (b) Amplitude-normalized photobleaching dynamics of fluorescence of single SPASER nanoparticle in comparison with the fluorescence of Cy 7.5 dye molecules in water.

Figure 3. Detection of single SARS-CoV-2 viral particles via measurement of SPASER nanoparticles fluorescence attached to virions through SARS-CoV-2 antibodies: (a) white-light image of dried out a droplet with added SPASER nanoparticles into it; (b) fluorescent image of the same droplet under 780 nm laser light excitation, orange arrows indicate antibodies' agglomerates, red arrows indicates SARS-CoV-2 viral particles; (c) cross-sections of fluorescent images of antibodies agglomerates (orange line), pseudo viral particle, having about 5 time less number of spike molecules (black line), SARS-CoV-2 viral particle (red line).